HAL
open science

A polarimetric study of asteroids in comet-like orbits

Jooyeon Geem, Masateru Ishiguro, Yoonsoo P. Bach, Daisuke Kuroda, Hiroyuki Naito, Hidekazu Hanayama, Yoonyoung Kim, Yuna G. Kwon, Sunho Jin, Tomohiko Sekiguchi, et al.

▶ To cite this version:

Jooyeon Geem, Masateru Ishiguro, Yoonsoo P. Bach, Daisuke Kuroda, Hiroyuki Naito, et al.. A polarimetric study of asteroids in comet-like orbits. Astronomy and Astrophysics - A&A, 2022, 658, 10.1051/0004-6361/202142014 . insu-03718989

HAL Id: insu-03718989

https://insu.hal.science/insu-03718989v1

Submitted on 11 Jul 2022

HAL is a multi-disciplinary open access archive for the deposit and dissemination of scientific research documents, whether they are published or not. The documents may come from teaching and research institutions in France or abroad, or from public or private research centers.

L'archive ouverte pluridisciplinaire **HAL**, est destinée au dépôt et à la diffusion de documents scientifiques de niveau recherche, publiés ou non, émanant des établissements d'enseignement et de recherche français ou étrangers, des laboratoires publics ou privés.

A&A 658, A158 (2022)
https://doi.org/10.1051/0004-6361/202142014
© ESO 2022

Astronomy & Astrophysics

A polarimetric study of asteroids in comet-like orbits*

Jooyeon Geem[1,2], Masateru Ishiguro[1,2], Yoonsoo P. Bach[1,2], Daisuke Kuroda[3], Hiroyuki Naito[4], Hidekazu Hanayama[5], Yoonyoung Kim[6], Yuna G. Kwon[6], Sunho Jin[1,2], Tomohiko Sekiguchi[7], Ryo Okazaki[7], Jeremie J. Vaubaillon[8], Masataka Imai[9], Tatsuharu Oono[10], Yuki Futamura[10], Seiko Takagi[10], Mitsuteru Sato[10], Kiyoshi Kuramoto[10], and Makoto Watanabe[11]

[1] Department of Physics and Astronomy, Seoul National University, 1 Gwanak, Seoul 08826, Republic of Korea
[2] SNU Astronomy Research Center, Seoul National University, 1 Gwanak-ro, Gwanak-gu, Seoul 08826, Republic of Korea
e-mail: geem@astro.snu.ac.kr; ishiguro@astro.snu.ac.kr
[3] Okayama Observatory, Kyoto University, 3037-5 Honjo, Kamogata, Asakuchi, Okayama 719-0232, Japan
[4] Nayoro Observatory, 157-1 Nisshin, Nayoro, Hokkaido 096-0066, Japan
[5] Ishigakijima Astronomical Observatory, National Astronomical Observatory of Japan, 1024-1 Arakawa, Ishigaki, Okinawa 907-0024, Japan
[6] Institut für Geophysik und Extraterrestrische Physik, Technische Universität Braunschweig, Mendelssohnstr. 3, 38106 Braunschweig, Germany
[7] Asahikawa Campus, Hokkaido University of Education, Hokumon, Asahikawa, Hokkaido 070-8621, Japan
[8] Observatoire de Paris, I.M.C.C.E., Denfert Rochereau, Bat. A., 75014 Paris, France
[9] Faculty of Science, Kyoto Sangyo University, Banyukan B401, Motoyama, Kamigamo, Kita-Ku, Kyoto-shi, Kyoto 603-8555, Japan
[10] Department of Cosmosciences, Graduate School of Science, Hokkaido University, Kita-ku, Sapporo, Hokkaido 060-0810, Japan
[11] Department of Applied Physics, Okayama University of Science, 1-1 Ridai-cho, Kita-ku, Okayama, Okayama 700-0005, Japan

Received 13 August 2021 / Accepted 1 October 2021

ABSTRACT

Context. Asteroids in comet-like orbits (ACOs) consist of asteroids and dormant comets. Due to their similar appearance, it is challenging to distinguish dormant comets from ACOs via general telescopic observations. Surveys for discriminating dormant comets from the ACO population have been conducted via spectroscopy or optical and mid-infrared photometry. However, they have not been conducted through polarimetry.

Aims. We conducted the first polarimetric research of ACOs.

Methods. We conducted a linear polarimetric pilot survey for three ACOs: (944) Hidalgo, (3552) Don Quixote, and (331471) 1984 QY1. These objects are unambiguously classified into ACOs in terms of their orbital elements (i.e., the Tisserand parameters with respect to Jupiter T_J significantly less than 3). Three ACOs were observed by the 1.6 m Pirka Telescope from UT 2016 May 25 to UT 2019 July 22 (13 nights).

Results. We found that Don Quixote and Hidalgo have polarimetric properties similar to comet nuclei and D-type asteroids (optical analogs of comet nuclei). However, 1984 QY1 exhibited a polarimetric property consistent with S-type asteroids. We conducted a backward orbital integration to determine the origin of 1984 QY1, and found that this object was transported from the main belt into the current comet-like orbit via the 3:1 mean motion resonance with Jupiter.

Conclusions. We conclude that the origins of ACOs can be more reliably identified by adding polarimetric data to the color and spectral information. This study would be valuable for investigating how the ice-bearing small bodies distribute in the inner Solar System.

Key words. techniques: polarimetric – minor planets, asteroids: individual: (944) Hidalgo – minor planets, asteroids: individual: (3552) Don Quixote – minor planets, asteroids: individual: (331471) 1984 QY1

1. Introduction

A classification between comets and asteroids (the notation is given in Appendix A) is important for investigating the compositional distribution in the present Solar System. In a conventional view, asteroids are distributed in the inner Solar System (i.e., mostly located in the main-belt region with low eccentricities), while comets originate from the outer Solar System (the Kuiper Belt or the Oort Cloud) with high eccentricities.

Because of their different origins, asteroids and comets have been conventionally distinguished by several properties. In terms of appearance, comets show tails and comae by ejecting gas and dust as they approach the Sun. Asteroids generally do not show cometary activity (except active asteroids, Jewitt 2012), so they have a point-source appearance. In terms of the orbital properties, the Tisserand parameter (an approximation derived from the Jacobi integral of the circular restricted three-body problem) with respect to Jupiter (T_J) has been employed to discriminate between comets and asteroids. In general, asteroids are dynamically disconnected from Jupiter, while comets are coupled or intersect with the orbit of Jupiter, providing $T_J > 3$ for asteroids and $T_J < 3$ for comets (Kresak 1982; Levison & Duncan 1997).

* Processed data (FITS) and lightcurves (data under Fig. B.1) are only available at the CDS via anonymous ftp to cdsarc.u-strasbg.fr (130.79.128.5) or via http://cdsarc.u-strasbg.fr/viz-bin/cat/J/A+A/658/A158

Table 1. Orbits and spectral types of our targets.

Target name	a [(a)] (au)	e [(b)]	i [(c)] (deg)	T_J [(d)]	Spectral type	References
QY1	2.50	0.89	14.3	2.68	Unidentified (S_q or Q)[(e)]	...
Don Quixote	4.26	0.71	31.1	2.31	D	1, 2
Hidalgo	5.73	0.66	42.5	2.07	D	2

Notes. [(a)]Semimajor axis, [(b)]eccentricity, [(c)]inclination, [(d)]tisserand parameter with respect to Jupiter, [(e)]see Sect. 4.3. We obtained these orbital elements (a, e, and i) from the web-based JPL Small-Body Database Browser (`https://ssd.jpl.nasa.gov/sbdb.cgi`).
References. (1) Binzel et al. (2004); (2) Tholen & Barucci (1989).

In terms of the optical properties, reflectance spectra and geometric albedos (p_V) are used for classification (Licandro et al. 2008, 2011; Kim et al. 2014; DeMeo & Binzel 2008). Typically, comet nuclei have red spectra with low p_V (p_V = 0.02–0.06, Campins & Fernández 2002; Lamy et al. 2004), and asteroids have a wide range of reflectance spectra and geometric albedos (p_V = 0.02–0.60, Usui et al. 2011). However, it turns out that this conventional classification could not work for some objects, such as asteroids in comet-like orbits (i.e., asteroids having apparent $T_J < 3$, hereafter ACOs).

Although dormant comets in the ACO population have been investigated via several methods, such as optical multiband photometry, spectroscopy, and infrared photometry (Fernández et al. 2001, 2005; Kim et al. 2014), few have been studied through polarimetry. Polarimetric observations can provide the polarization degree–phase angle $P_r(\alpha)$ profile of targets, where α is the Sun–target–observer angle. In general, the $P_r(\alpha)$ profiles of small bodies in the Solar System show negative P_r (i.e., light polarized in a parallel direction to the scattering plane) at $\alpha \lesssim \alpha_0$ and positive P_r (i.e., the perpendicularly polarized direction with respect to the scattering plane) at $\alpha \geq \alpha_0$ (Cellino et al. 2016). Here, α_0 is the inversion angle where $P_r(\alpha_0) = 0$ is established, and which generally appears at $\alpha \sim 20°$. Then, P_r pseudolinearly increases around α_0 with a slope of h and shows the maximum polarization degree (P_{max}) at $\alpha_{max} \sim 100°$. Consequently, the $P_r(\alpha)$ profiles are characterized by several key parameters (e.g., the slope h, α_0, P_{max}). The surface properties (such as albedo and grain size) were conjectured with these parameters (Geake & Dollfus 1986; Dollfus et al. 1989; Shkuratov & Opanasenko 1992; Lupishko 2018).

In this paper we conducted a polarimetric pilot survey of three ACOs, (944) Hidalgo, (3552) Don Quixote, and (331471) 1984 QY1 (hereafter Hidalgo, Don Quixote, and QY1), to test the potential of polarimetry for ACO research. We chose Don Quixote and QY1 not only because they were bright in 2016–2019, but also because they have a high probability of being Jupiter-family comets (>96%, Bottke et al. 2002). Hidalgo is a dormant comet candidate because of its orbital and spectral properties (Hartmann et al. 1987; Tholen 1984). More detailed information on the targets is summarized in Table 1. We describe the observations and data reduction processes in Sect. 2 and observational results in Sect. 3. We discuss the results based on our polarimetry and the dynamical properties and the surface prospects of the polarimetric study for ACOs in Sect. 4.

2. Observations and data analysis

The journal of the observations is given in Table 2. We conducted polarimetry with the 1.6-m Pirka Telescope at the Hokkaido University Observatory (142.°5 E, 44.°4 N at 151 m above sea level, observatory code number Q33) in Japan from UT 2016 May 25 to 2019 July 22. During this period there were three ACOs (Don Quixote, Hidalgo, and QY1) that were bright enough to be measured by the instruments (V-band magnitudes $\lesssim$17 mag) with sufficiently small errors ($\lesssim$1%) at moderately large $\alpha \sim 30°$. Among them, we had an opportunity to observe QY1 at a very large α ($\alpha \approx 100°$). We utilized the visible multispectral imager (MSI) attached to the Cassegrain focus of the 1.6-m Pirka telescope, covering a field of view of $3.'3 \times 3.'3$ with a pixel resolution of 0.″39 (Watanabe et al. 2012). We obtained the polarimetric data with V-band and R_C-band filters. The polarimetric module is optional for MSI, which consists of a rotatable half-wave plate and a Wollaston prism (a polarizing beam splitter), which has the advantage of reducing the influence of time-dependent atmospheric extinction. A polarization mask divides the field of view into two areas of the sky of $3.'3 \times 0.'7$, and each area produces a data set having ordinary and extraordinary images simultaneously without mixing ordinary and extraordinary signals (Fig. 1). We adjusted an exposure time of 60–180 s, considering the signal-to-noise ratio at each half-wave plate angle (changed in the sequence of $\theta = 0°, 45°, 22.°5$, and 67.°5).

We analyzed the data in the same manner as in Ishiguro et al. (2017) and other papers using Pirka/MSI (Kuroda et al. 2015, 2021). The raw data were bias-subtracted and flat-fielded using the MSI data reduction package. Cosmic rays were subtracted using the `L.A. Cosmic` tool (van Dokkum 2001). After preprocessing, we performed aperture photometry to extract the source fluxes from the ordinary and extraordinary parts of objects on the images using the photometry package in the Image Reduction and Analysis Facility (`IRAF`) and `astropy` (Astropy Collaboration 2013, 2018) of the Python package. The typical aperture size was 2.″73–5.″85. Additionally, by visual inspection, we excluded the images with background objects within an aperture radius from the center of our targets.

We obtained the linear polarization degree (P) and the position angle (θ_P) with the equations

$$P = \sqrt{\left(\frac{Q}{I}\right)^2 + \left(\frac{U}{I}\right)^2} \tag{1}$$

and

$$\theta_P = \frac{1}{2}\tan^{-1}\left(\frac{U}{Q}\right), \tag{2}$$

where I, Q, and U are the Stokes parameters derived from the extracted fluxes (Tinbergen 1996), and θ_P denotes the polarization position angle with respect to the celestial north. Before

Table 2. Observation circumstance.

Target name	Date	UT	Filter	Exptime [(a)] (s)	N [(b)]	r [(c)] (au)	Δ [(d)] (au)	α [(e)] (deg)	ϕ [(f)] (deg)
QY1	2016-May-25	12:09–17:20	R_C	120–180	28	0.87	0 30	111.7	42.2
	2016-May-27	13:22–14:40	V	120	20	0.90	0.28	104.8	60.6
	2016-May-27	12:53–14:19	R_C	120	24	0.90	0.28	104.8	60.5
	2016-May-28	12:55–15:42	V	120	28	0.92	0.28	101.0	74.0
	2016-May-28	13:35–16:26	R_C	120	28	0.92	0.28	101.0	74.5
	2016-May-29	12:58–16:29	V	120	28	0.94	0.28	97.1	89.1
	2016-May-29	12:50–16:16	R_C	120	20	0.94	0.28	97.1	89.3
	2016-Jun-21	12:54–14:38	V	60	60	1.33	0.52	43.4	131.3
	2016-Jun-21	11:25–17:24	R_C	60–120	56	1.33	0.52	43.4	131.3
	2016-Jun-24	11:20–14:56	R_C	60–120	32	1.38	0.58	41.2	128.8
Don Quixote	2018-Jul-24	17:18–18:09	R_C	120–180	20	1.58	1.46	38.7	254.0
	2018-Aug-28	15:57–16:16	R_C	60	20	1.86	1.40	32.5	248.4
	2018-Sep-01	14:53–18:18	R_C	60	88	1.89	1.40	31.5	246.5
	2018-Sep-02	15:57–17:41	I_C	120	36	1.90	1.40	31.2	246.0
Hidalgo	2018-Sep-01	17:13–17:59	R_C	60	32	2.02	1.90	29.6	266.5
	2019-Apr-19	13:15–13:59	R_C	120	24	3.52	4.49	22.9	119.0
	2019-May-30	12:13–13:05	R_C	120	24	2.82	2.92	20.3	105.4
	2019-Jul-22	11:18–11:43	R_C	120	12	10.93	3.79	13.1	93.9

Notes. [(a)] Exposure time for each image in sec, [(b)] number of exposures used to obtain polarimetric parameters, [(c)] median heliocentric distance in au, [(d)] median geocentric distance in au, [(e)] median solar phase angle in deg, [(f)] position angle of the scattering plane in deg. The web-based JPL Horizons system (`http://ssd.jpl.nasa.gov/?horizons`) was used to obtain these quantities.

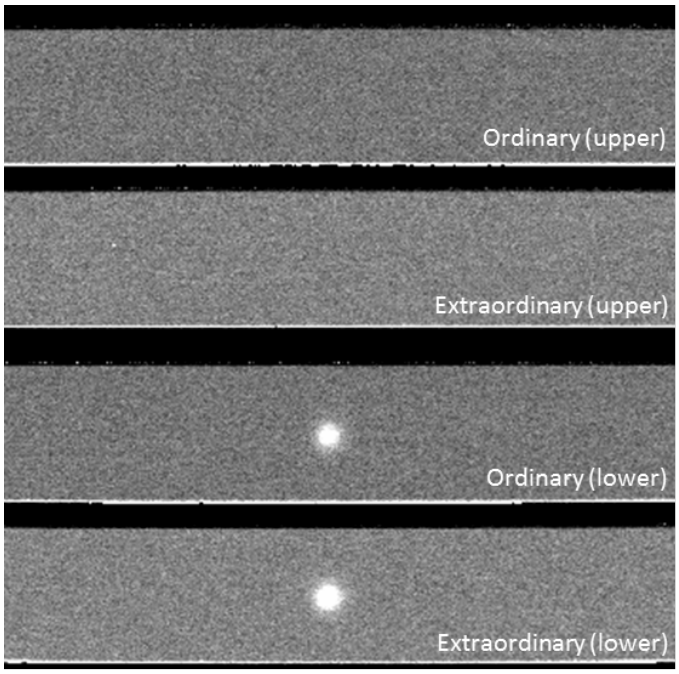

Fig. 1. Example of a preprocessed polarimetric image of QY1 taken in the R_C-band with an exposure time of 120 s. The field of view is split into two regions (*upper* and *lower*) by the polarization mask (see Sect. 2).

deriving P and θ_P in the above equations, we corrected the polarization efficiency, instrumental polarization, and position angle offset at the given wavelengths (Ishiguro et al. 2017). After the calibration, we calculated the weighted mean of q and u on each date and derived the polarimetric result. To consider the influence of random noise in P, we applied the following equation (Wardle & Kronberg 1974):

$$P' = \sqrt{P^2 - \sigma_P^2}. \tag{3}$$

When P is nearly equal to zero, σ_P^2 inevitably becomes larger than P^2, which makes the value in the root negative. In this case, we regard it as $P = 0\%$.

Finally, we converted a polarization degree with respect to the scattering plane (the plane constituted by the target, the Sun, and the Earth) with the equations

$$P_r = P' \cos(2\theta_r) \tag{4}$$

and

$$\theta_r = \theta_P - (\phi \pm 90^\circ), \tag{5}$$

where ϕ is the position angle referring to the scattering plane on the sky and θ_r is the angle between the measured direction of the strongest electric vector and the normal to the Sun–target–observer plane, following the convention of asteroids and comet polarimetry (e.g., Lupishko 2014). The $\pm$ sign in parentheses is chosen to satisfy $0^\circ \leq (\phi \pm 90^\circ) \leq 180^\circ$ (Chernova et al. 1993).

All the preprocessed polarimetric data used are available via CDS.

3. Results

Table 3 summarizes the weighted mean values of the nightly linear polarimetric result and Fig. 2 shows the polarization phase curve. In the following subsections we describe our findings.

Table 3. Polarimetric results.

Target name	Date	UT	Filter	α (deg)	P [(a)] (%)	σP [(b)] (%)	θ_P [(c)] (deg)	$\sigma\theta_P$ [(d)] (deg)	P_r [(e)] (%)	θ_r [(f)] (deg)
QY1	2016-May-25	12:09–17:20	R_C	111.7	8.48	1.08	−50.95	3.64	8.45	−2.63
	2016-May-27	13:22–14:40	V	104.8	8.00	0.31	−31.94	1.12	7.97	−2.63
	2016-May-27	12:53–14:19	R_C	104.8	7.97	0.21	−32.76	0.75	7.92	−3.33
	2016-May-28	12:55–15:42	V	101.0	8.56	0.33	−19.56	1.09	8.56	−4.14
	2016-May-28	13:35–16:26	R_C	101.0	8.48	0.27	−17.20	0.90	8.46	−1.88
	2016-May-29	12:58–16:29	V	97.1	7.72	0.24	−4.74	0.90	7.65	−3.85
	2016-May-29	12:50–16:16	R_C	97.1	7.64	0.27	−2.19	0.99	7.63	−1.56
	2016-Jun-21	12:54–14:38	V	43.4	2.88	0.35	42.45	3.48	2.88	1.14
	2016-Jun-21	11:25–17:24	R_C	43.3	2.75	0.38	38.06	3.98	2.73	−3.25
	2016-Jun-24	11:20–14:56	R_C	41.2	2.32	0.55	32.27	6.81	2.26	−6.56
Don Quixote	2018-Jul-24	17:18–18:09	R_C	38.7	7.64	0.37	−21.48	1.39	7.50	−5.50
	2018-Aug-28	15:57–16:16	R_C	32.5	4.65	0.71	−30.40	4.39	4.43	−8.80
	2018-Sep-01	14:53–18:18	R_C	31.5	3.72	0.44	−23.74	3.41	3.72	−0.25
	2018-Sep-02	15:57–17:41	I_C	31.2	4.16	0.63	−20.19	4.32	4.12	3.85
Hidalgo	2018-Sep-01	17:13–17:59	R_C	29.6	3.47	0.12	−5.52	0.97	3.46	−1.99
	2019-Apr-19	13:15–13:59	R_C	22.9	1.16	0.14	23.45	3.49	1.14	−5.51
	2019-May-30	12:13–13:05	R_C	20.3	0	0.31	−11.80	49.49	0	−27.22
	2019-Jul-22	11:18–11:43	R_C	13.1	0.91	0.51	−86.37	16.03	−0.91	89.75

Notes. [(a)]Nightly averaged linear polarization degree in percent, [(b)] error of P in percent, [(c)] position angle of the strongest electric vector in deg, [(d)] error of θ_P in deg, [(e)] polarization degree referring to the scattering plane in percent (see Eq. (3)), [(f)] position angle referring to the scattering plane in deg (see Eq. (4)).

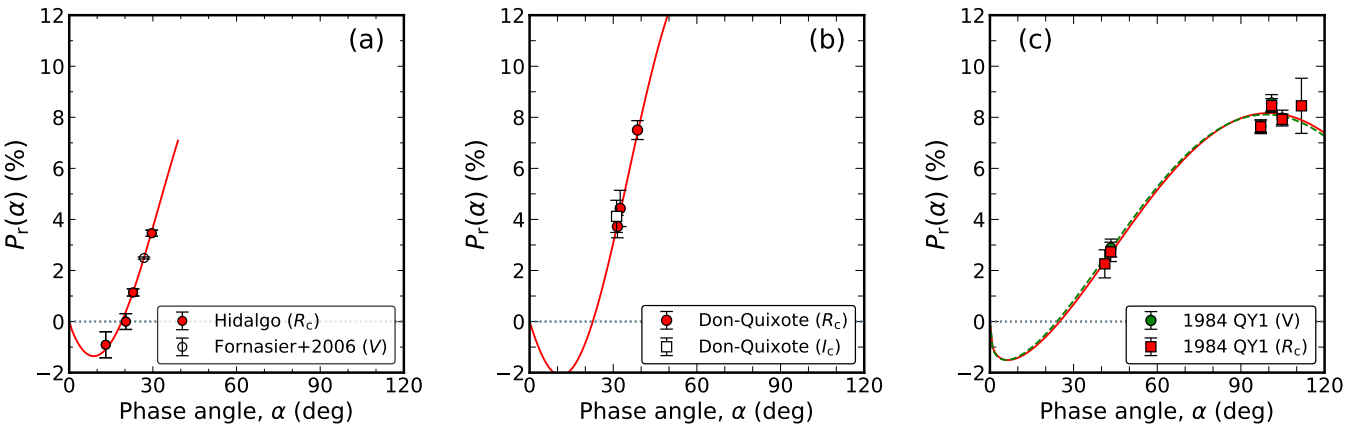

Fig. 2. Phase angle dependence of nightly averaged P_r for three ACOs: (*a*) Hidalgo, (*b*) Don Quixote, and (*c*) QY1. Polarization phase curves using the median of the Monte Carlo samples are shown as the red solid line for R_C band and the green dashed line for V band by using Eq. (6). For Hidalgo we plot the V-band data (open circle) from Fornasier et al. (2006).

3.1. Characterization of polarization phase curves

To capture the outlines of polarization phase curves, we fit the data using the empirical Lumme–Muinonen function (Lumme & Muinonen 1993; Penttilä et al. 2005). It is given as

$$P_r(\alpha) = h\left(\frac{\sin(\alpha)}{\sin(\alpha_0)}\right)^{c_1}\left(\frac{\cos\left(\frac{\alpha}{2}\right)}{\cos\left(\frac{\alpha_0}{2}\right)}\right)^{c_2}\sin(\alpha-\alpha_0)\,, \tag{6}$$

where α_0, h, c_1, and c_2 are free parameters for fitting polarization phase curves. We modify the original Lumme–Muinonen function so that h corresponds to the polarimetric slope at $\alpha = \alpha_0$. We fit the observation data with Eq. (6), employing the Markov chain Monte Carlo (MCMC) method in `emcee` (Foreman-Mackey et al. 2013, version 3.0.2). We set boundary conditions of $0 < h < 1$, $0 < c_1, c_2 < 10$, and $10° < \alpha_0 < 40°$. The uncertainties of best-fit parameters are derived based on the 16th, 50th, and 84th percentiles of the samples in the marginalized distributions. The script to fit the polarization phase curve is available via the GitHub[1]. The best-fit parameters with $\pm 1\sigma$ uncertainties are summarized in Table 4. With the parameters we show the fitted profiles in Fig. 2. In the figure the polarization phase curves of Don Quixote and Hidalgo are similar to each other, but are different from QY1 in that they have polarimetric slopes steeper than QY1 (i.e., larger h values). The inversion angle of Hidalgo is determined well to $\alpha_0 = 18\overset{\circ}{.}87^{+0.62}_{-0.84}$. On the contrary, the inversion angles of Don Quixote and QY1 were less precise due to the lack of data in the negative branch, preventing accurate

[1] https://github.com/Geemjy/Geem_2021_AA

Table 4. Fitting result of polarization phase curves.

Target name	Filter	h (%/deg)	α_0 (deg)	c_1	c_2	$\alpha_{\max}$ (deg)	$P_{\max}$ (%)
Hidalgo	R_C	$0.253^{+0.047}_{-0.056}$	$18.87^{+0.62}_{-0.84}$	$0.892^{+0.418}_{-0.351}$	$5.429^{+3.178}_{-3.570}$	...	...
Don Quixote	R_C	$0.353^{+0.223}_{-0.198}$	$22.79^{+2.51}_{-3.70}$	$1.017^{+0.871}_{-0.696}$	$5.394^{+3.153}_{-3.535}$	...	...
QY1	V	$0.129^{+0.042}_{-0.050}$	$24.05^{+4.24}_{-4.80}$	$0.323^{+0.402}_{-0.233}$	$0.377^{+0.456}_{-0.267}$	$98.83^{+5.91}_{-5.28}$	$8.08^{+3.19}_{-3.11}$
QY1	R_C	$0.127^{+0.043}_{-0.052}$	$24.87^{+4.03}_{-4.68}$	$0.341^{+0.444}_{-0.248}$	$0.347^{+0.406}_{-0.250}$	$99.79^{+5.77}_{-5.26}$	$8.14^{+3.41}_{-3.55}$

Table 5. Results of α_0, h, and p_V.

Target name	α_0 (deg)	h (%/deg)	p_V	References
Hidalgo	$18.87^{+0.62}_{-0.84}$ [(a)]	$0.253^{+0.047}_{-0.056}$ [(a)]	$0.050^{+0.017}_{-0.009}$ [(b)]	...
Don Quixote	$22.79^{+2.51}_{-3.70}$ [(a)]	$0.353^{+0.223}_{-0.198}$ [(a)]	$0.035^{+0.049}_{-0.014}$ [(b)]	...
QY1	$24.87^{+4.03}_{-4.68}$ [(c)]	$0.129^{+0.042}_{-0.050}$ [(c)]	$0.153^{+0.107}_{-0.042}$ [(b)]	...
S-type asteroids	20.7 ± 0.2 [(c)]	0.110 ± 0.005 [(c)]	0.21 ± 0.08	1, 2
D-type asteroids	18.2 ± 0.3 [(c)]	0.341 ± 0.109 [(c)]	0.09 ± 0.05	1, 2
C-type asteroids	19.4 ± 0.1 [(c)]	0.387 ± 0.037 [(c)]	0.07 ± 0.04	1, 2
Comet nuclei	...	...	$0.02 \sim 0.06$	3

Note. [(a)] Derived by the observation in R_C band. [(b)] These p_V values were derived from h and color. [(c)] Derived by the observation in V band.
References. (1) Belskaya et al. (2017); (2) Usui et al. (2013); (3) Lamy et al. (2008).

determination (see Table 5), and yet the fitting process would work well because these α_0 values are typical of general asteroids (i.e., ~20°).

Figure 3 compares the polarization phase curves of three ACOs with a comet nucleus and other types of asteroids. We utilize the P_r data of a bare comet nucleus (209P/LINEAR, Kuroda et al. 2015) and C-, D-, B-, and S-type asteroids (Gil-Hutton et al. 2014, 2017; Ishiguro et al. 2017; Ito et al. 2018; Kuroda et al. 2021; Lupishko 2014; Shinnaka et al. 2018).

In Fig. 3, the distribution of different objects depends mostly on their albedos. Lower albedo objects are distributed on the upper side, while higher albedo objects are distributed on the lower side. We draw the borderline corresponding to $p_V = 0.1$ (dash-dotted line) in Fig. 3. The borderline is the straight line whose slope is obtained by putting $p_V = 0.1$ in Eq. (7) and starts from $\alpha = 20°$ (i.e., typical α_0 of asteroids, Belskaya et al. 2017). It becomes clear that objects with $p_V < 0.1$ are located above the borderline. The P_r of Don Quixote, Hidalgo, and the comet nucleus are located on the upper side, indicating that they have consistent albedo values ($p_V < 0.1$). On the other hand, the polarimetric profile of QY1 is similar to that of S-type asteroids as it is below the line for $p_V = 0.1$.

3.2. Derivation of geometric albedo

Since the polarimetric slopes depend on their albedo, as seen in Sect. 3.1, we derive the geometric albedos (p_V) of ACOs from their slope h. It is well known that the slope h has a good correlation with p_V. This was first noted by Widorn (1967) and Kenknight et al. (1967). The correlation is expressed with the empirical equation

$$\log_{10}(p_V) = C_1 \log_{10}(h) + C_2, \tag{7}$$

where C_1 and C_2 are constants. They have been determined by several research groups (Masiero et al. 2012; Cellino et al. 2015; Lupishko 2018). Here we use $C_1 = -1.016 \pm 0.010$ and $C_2 = -1.719 \pm 0.012$ from Lupishko (2018), which uses the most comprehensive data sets obtained by infrared space telescopes and occultations. In addition, although C_1 and C_2 are obtained in V band, we practically assume that the slope h is dominantly controlled by the geometric albedo regardless of wavelength (Umow 1905) to apply C_1 and C_2 to our data in R_C band. Substituting the slope h values in Eq. (7), we computed the geometric albedo values; and the results are summarized in Table 5. The uncertainty of the albedo is calculated based on the uncertainties of h, C_1, and C_2 in Eq. (7). For comparison, we provide the average values or typical range of asteroids and comet nuclei in Table 5.

In the case of Don Quixote and Hidalgo, only geometric albedos in the R_C band (p_{R_C}) are derived from our polarimetry. The results are $p_{R_C} = 0.055^{+0.077}_{-0.023}$ for Don Quixote and $p_{R_C} = 0.078^{+0.032}_{-0.015}$ for Hidalgo. Since the geometric albedo is defined in the V band, we should convert them (i.e., p_{R_C}) to V-band albedos (i.e., p_V) using their color indices ($V - R$). The applied $V - R$ values are summarized in Appendix C. The corresponding p_V values are summarized in Table 5. These p_V values of Don Quixote and Hidalgo are in the range of the typical p_V of comet nuclei and C- and D-type asteroids (Lamy et al. 2008; Usui et al. 2013). In contrast, p_V of QY1 is in the range of typical p_V of S-type asteroids (Usui et al. 2013).

We note that slope h of Don Quixote and QY1 are derived by extrapolation to the range of $\alpha < 20°$ where no data is available. Because Eq. (6) used for the fittings is the empirical function (Lumme & Muinonen 1993; Penttilä et al. 2005), polarimetric parameters derived by extrapolation is uncertain. However, we confirm that, while their $\alpha_0 > 15°$, Don Quixote always shows the slope h and the albedo (i.e., $p_V < 0.1$) compatible with those of D-type asteroids (the optical analog of comet nuclei), whereas QY1 indicates these values are comparable with those of S-type asteroids.

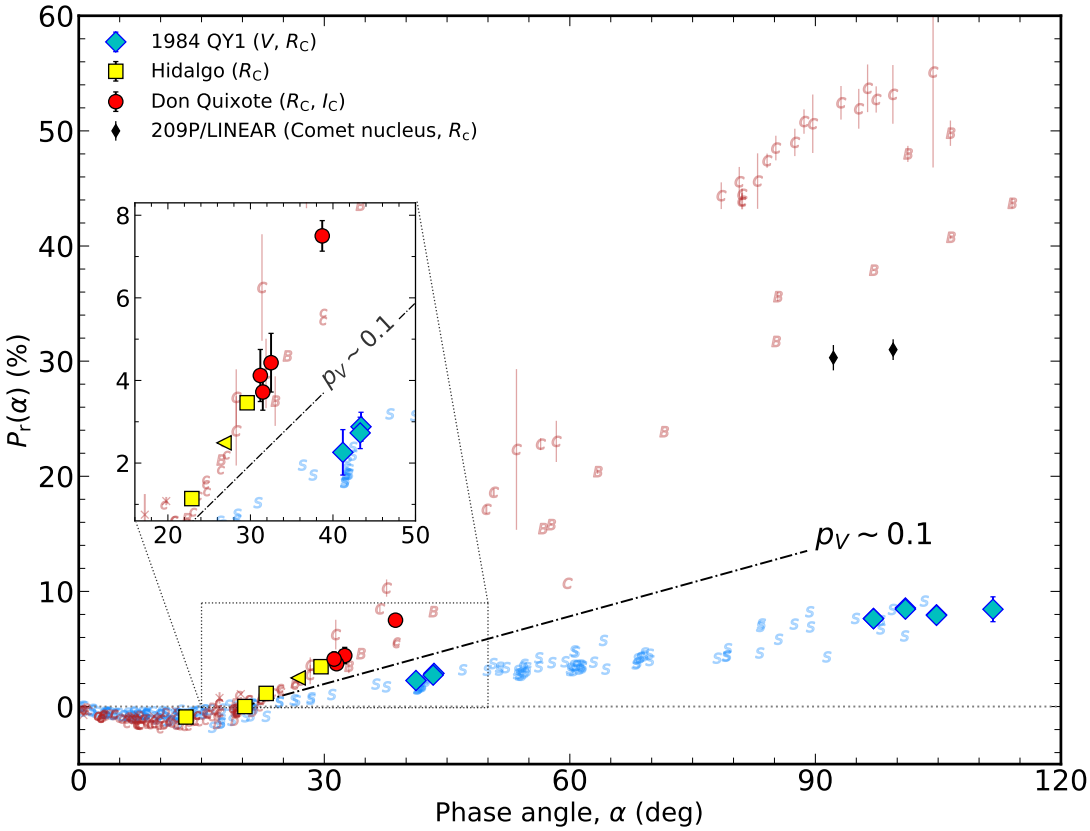

Fig. 3. Comparison of $P_r(\alpha)$ profiles of QY1, Don Quixote, and Hidalgo with asteroids and a bare comet nucleus, 209P/LINEAR, (Kuroda et al. 2015). Each letter (C, B, and S) indicates the taxonomic types. The P_r value of Hidalgo in Fornasier et al. (2006) is plotted as the triangle marker. We plot the diagnostic line (dash-dotted line) corresponding to $p_V = 0.1$. Objects with $p_V \leq 0.1$ are be located on the upper side of the line and vice versa.

3.3. Slope h and the color Index V–R

Although the polarimetric slope h is a useful proxy of albedo, it is insufficient to distinguish possible dormant comets from C-complex asteroids (C-, F-, and B-types) because comet nuclei (including D-type) and C-complex asteroids have similar albedo values. Therefore, we utilize the color index $V - R$ together with the slope h. We compare the slopes h and $V - R$ of ACOs with those of other asteroids and comet nuclei (Fig. 4). We convert the slope h of Don Quixote and Hidalgo in the R_C band to the V band using their $V - R$ color indices (Appendix C). In Fig. 4, objects are divided into three major groups: S-type asteroids; C-, F-, and B-type asteroids; and comet nuclei. Because comet nuclei have optical properties (colors and albedos) similar to D-type asteroids, they overlap with each other. Don Quixote and Hidalgo are clearly distinguished from C-type asteroids and are located in a region similar to comet nuclei and D-type asteroids. Meanwhile, QY1 is compatible with S-type asteroids.

4. Discussion

In this study we attempt to extract dormant comets from the ACO list. We conduct a polarimetric pilot survey for three ACOs to test the potentiality and found that two are likely dormant comets, while another is an S-type asteroid. Here we describe the characteristics of these three ACOs in the following subsections.

4.1. (3552) Don Quixote

Don Quixote should be in the class of comets of outer Solar System origin that contain volatile components such as H_2O and CO_2 ices. This object was discovered in 1983 as an asteroid despite the comet-like orbit ($T_J < 3$, Weissman et al. 2002). It has a very elongated orbit with perihelion and aphelion distances of 1.24 au and 7.28 au, respectively. The diameter and geometric albedo are estimated as $D = 18.4^{+0.3}_{-0.4}$ km and $p_V = 0.03^{+0.02}_{-0.01}$ from thermal infrared data taken with the *Spitzer* Space Telescope, the NASA Infrared Telescope Facility, and the Wide-field Infrared Survey Explorer (WISE) (Mommert et al. 2014). It is classified as a D-type asteroid (Tholen 1984; Bus & Binzel 2002; Rayner et al. 2003). Recent telescopic observations at optical and infrared wavelengths confirm that Don Quixote has exhibited weak comet-like activity at heliocentric distances within 3 au (Mommert et al. 2014, 2020; Kokhirova et al. 2021). The activities were not episodic but recurrent, as observed at different perihelion passages in 2009 and 2017–2018. Moreover, a coma and a tail show the excess signal associated with CO_2 molecules in the *Spitzer* Space Telescope observation (Mommert et al. 2014). For these reasons, there is no doubt that Don Quixote is a volatile-bearing cometary object of outer Solar System origin.

Our polarimetric observation was conducted starting on July 24, 2018, ten days after the cessation of activity was confirmed by Kokhirova et al. (2021). We thus measure the polarization degree of the bare nucleus. Without using a space infrared telescope or a large telescope with a mid-infrared instrument, we derive the albedo of $p_V = 0.035^{+0.049}_{-0.014}$, which is consistent with the result from the *Spitzer* Space Telescope (Mommert et al. 2014). The comet-like optical properties are seen in the polarimetric slope–color plot (Fig. 4). The polarimetry of Don Quixote thus becomes a benchmark for demonstrating the validity of

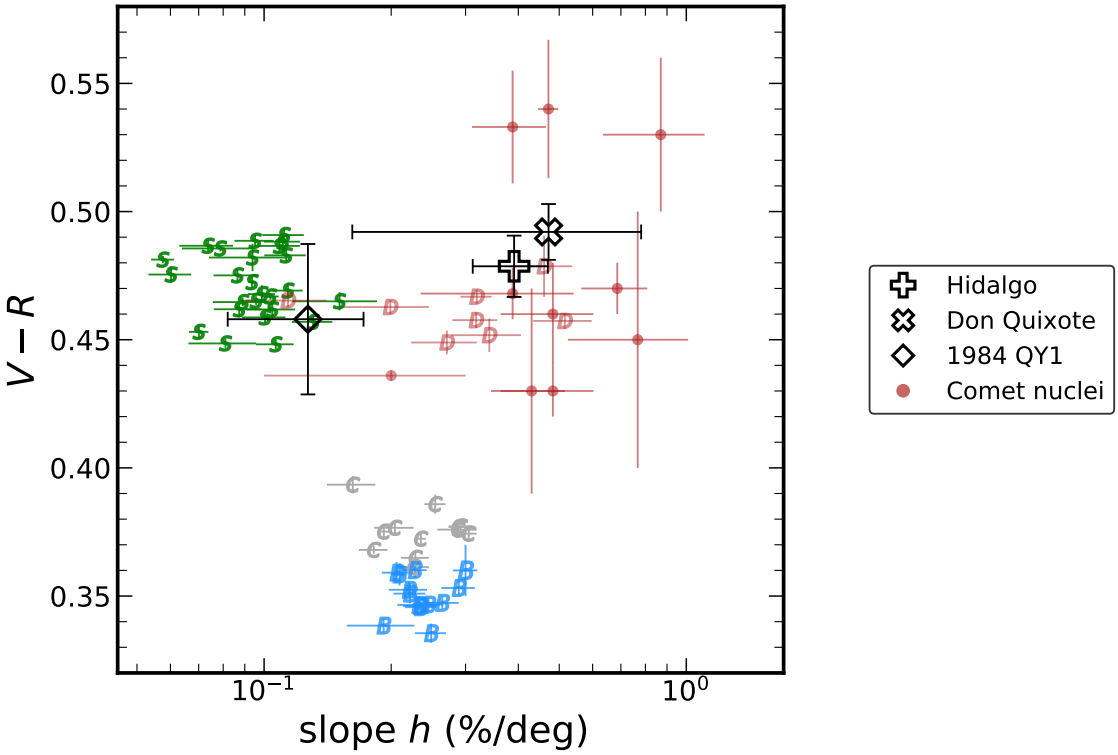

Fig. 4. Polarimetric slope h and $V-R$ plot of Hidalgo, Don Quixote, and QY1 with different types of asteroids and comet nuclei. Each letter (C, B, S, and D) indicates the taxonomic asteroid type. We label (7968) Elst-Pizarro as a B-type asteroid (Licandro et al. 2011). More details and references are given in Sect. 3.3 and Appendix C.

dormant comet extraction using the polarimetric slope–color plot.

4.2. (944) Hidalgo

Since its discovery in 1920 Hidalgo has never exhibited comet-like activity. Nevertheless, it is suspected to be a dormant comet for the reasons described here. This object has a very elongated orbit with perihelion and aphelion distances of 1.95 au and 9.53 au. Thus, this object not only intersects Jupiter's orbit (the semimajor axis $a = 5.20$ au), but also reaches Saturn's orbit ($a = 9.55$ au) around its aphelion. The diameter and geometric albedo are estimated as $D = 61.4 \pm 12.7$ km and $p_V = 0.028 \pm 0.006$ using WISE data and $D = 52.45 \pm 3.60$ km (Licandro et al. 2016) and $p_V = 0.042 \pm 0.007$ using AKARI data (Usui et al. 2011). The albedo value we derived via polarimetry is $p_V = 0.050^{+0.017}_{-0.009}$. These result are in the albedo range of comet nuclei. Additionally, Hidalgo has a spectrum of D-type asteroids (Tholen 1984; Bus & Binzel 2002; Rayner et al. 2003). All the results support the idea that Hidalgo is a strong candidate for a dormant comet.

As shown in Table 3 and Fig. 2, Hidalgo is observed around $\alpha \sim 20°$, making it possible to derive the polarimetric inversion angle (α_0). From the fitting we derive $\alpha_0 = 18\overset{\circ}{.}87^{+0.62}_{-0.84}$. The derived α_0 of Hidalgo is slightly smaller than for the majority of asteroids, but consistent with the typical α_0 value of D-type asteroids (i.e., $\alpha_0 = 18\overset{\circ}{.}2 \pm 0\overset{\circ}{.}3$, Belskaya et al. 2017), strengthening the result that it is D-type. Meanwhile, there are two reports regarding the α_0 of objects showing comet-like activity derived without gas or dust contamination: 2P/Encke, which indicates $\alpha_0 \sim 13°$ in the R band (Boehnhardt et al. 2008), and (7968) Elst-Pizarro, which indicates $\alpha_0 = 17\overset{\circ}{.}6 \pm 2\overset{\circ}{.}1$ in the R band and $\alpha_0 = 17\overset{\circ}{.}0 \pm 1\overset{\circ}{.}6$ in the V band (Bagnulo et al. 2010). These α_0 values are smaller than typical asteroids and are nearer to F-type asteroids ($\alpha_0 \sim 15°$, Belskaya et al. 2005, 2017; Cellino et al. 2016).

Bagnulo et al. (2010) further note that three F-like asteroids, (4015) Wilson-Harrington (C- or F-type; Tholen 1984), (3200) Phaethon (B- or F-type; Tholen & Barucci 1989; Licandro et al. 2007), and (155140) 2005 UD (B- or F-type; Kinoshita et al. 2007), have evidence of dust emissions, and they point out the association between small α_0 asteroids and dust-ejecting objects. Although there are only two report (2P/Encke and (7968) Elst-Pizarro) that indicated the small α_0, it is interesting to study the small α_0 objects from the viewpoint of dust-ejecting objects. It is also a recent discovery that OSIRIS-REx witnesses dust ejection from (101955) Bennu (Lauretta et al. 2019). From polarimetry it is reported that the asteroid has a small α_0 (i.e., $\alpha_0 = 17\overset{\circ}{.}88 \pm 0\overset{\circ}{.}40$, Cellino et al. 2018).

In this paper, however, we consider that the application of α_0 may not be a decisive factor to distinguish comets (including dust-emitting objects) from asteroids. Because the purpose of this study is to discriminate icy cometary objects of outer Solar System origin from asteroidal objects, we should regard the small α_0 objects (7968) Elst-Pizarro (a Themis family member, Hsieh et al. 2004) and (101955) Bennu (an asteroid possibly originating from the Polana-Eulalia family complex, Bottke et al. 2015) as asteroids rather than comets. We note that our designations of comets and asteroids in this paper (Appendix A) do not contradict the idea of Bagnulo et al. (2010). As described in Belskaya et al. (2005), highly reflective particles with a size comparable to the optical wavelength may affect the small α_0 for 2P/Encke and (7968) Elst-Pizarro. As the number of α_0 measurements for dust-ejecting objects increases in the future, it is

Table 6. Orbital elements of QY1 at Epoch 2459396.5 (2021-07-01.0).

a [(a)] (au)	e [(b)]	i [(c)] (deg)	g [(d)] (deg)	n [(e)] (deg)	M [(f)] (deg)
2.500163	0.893873	14.282613	337.182719	142.265114	113.120460
$\pm 8.660 \times 10^{-9}$	$\pm 2.001 \times 10^{-8}$	$\pm 5.270 \times 10^{-6}$	$\pm 2.192 \times 10^{-5}$	$\pm 2.240 \times 10^{-5}$	$\pm 2.865 \times 10^{-6}$

Notes. [(a)] Semimajor axis in au, [(b)] eccentricity, [(c)] inclination in deg, [(d)] mean argument of perihelion in deg, [(e)] longitude of the ascending node in deg, [(f)] mean anomaly in deg. We obtained these elements from the web-based JPL Small-Body Database Browser (https://ssd.jpl.nasa.gov/sbdb.cgi).

expected that there may be a finding regarding the surface state of objects with small α_0.

Thus, it is very likely that Hidalgo is a dormant comet, even if it does not have a small α_0.

4.3. (331471) 1984 QY1

We conclude that QY1 is most likely an asteroid because of its high albedo ($p_V = 0.153^{+0.107}_{-0.042}$). The P_{max} value ($8.14^{+3.41}_{-3.55}$% in the R_C band) is significantly lower than that of the 209P/LINEAR nucleus. Recent SMASSII observation data indicate that QY1 is an S_q-type or Q-type asteroid when using the Bus-Demeo classification tool. The spectrum displays absorptions of approximately 0.9 and 1.9 µm, typical of these types of asteroids (DeMeo et al. 2009a; Rayner et al. 2003). Thus, these observations (including our polarimetry) indicate that QY1 is an S-complex asteroid.

The polarimetry of QY1 provides a rare opportunity for deriving the surface particle size. Taking advantage of our observations at large phase angles, we derive the particle size on QY1. It is known that P_{max} depends on the geometric albedo (Umow 1905) and the particle size (Geake & Dollfus 1986). Shkuratov & Opanasenko (1992) derived a formula to estimate the particle size d (in µm) from P_{max} and a sort of albedo:

$$d = 0.03 \exp\left(2.9\left(\log_{10}(100\,A) + 0.845 \log_{10}(10\,P_{max})\right)\right), \quad (8)$$

where A denotes an albedo at $\alpha = 5°$. Applying the intensity ratio ($I(0.°3)/I(5°) = 1.44 \pm 0.04$ for S-type asteroids; Belskaya & Shevchenko 2000), we obtain $A = 0.11 \pm 0.03$ for QY1. Substituting A in Eq. (8), we obtain an estimate of the particle diameter, $d \approx 70$ µm. The size is slightly larger than the S-type asteroid (4179) Toutatis ($\lesssim$50–80 µm, Ishiguro et al. 1997; Bach et al. 2019), but smaller than the near-Sun Q-type asteroid (1566) Icarus (100–130 µm, Ishiguro et al. 2017). We note that Eq. (8) should be applied to asteroids carefully since a formula is established on the lunar samples. Even so, we use Eq. (8), which is the same method as in previous studies for comparison.

Lastly, we consider the paradoxical problem that the S-type asteroid QY1 has a comet-like orbit. According to a dynamical study of near-Earth objects (Bottke et al. 2002), QY1 has a 96.1% probability of Jupiter-family comets origin, which was one of the highest-potential dormant comet candidates in the list. Since then, its orbital elements have been updated thanks to the accumulation of astrometric observations, yet QY1 has $T_J = 2.68$, which is significantly smaller than the criterion of $T_J = 3$. From the revised semimajor axis of $a = 2.497$ au we note that QY1 is in a 3:1 mean motion resonance (MMR) with Jupiter (i.e., $a_{3:1} = 2.50 \pm 0.03$ au). As pointed out in Kim et al. (2014) and Tancredi (2014), T_J must be treated carefully when considering origins. Main-belt asteroids in resonance should experience increasing orbital eccentricity to be transported into the near-Earth region (e.g., Morbidelli et al. 2002). QY1 has likely been injected into the current comet-like orbit by means of the 3:1 MMR with Jupiter. To confirm this hypothesis, we conduct a backward dynamical simulation of QY1 considering the gravity of eight planets and the Sun (Fig. 5). We employ the `Mercury 6` integrator for the simulation (Chambers 1999). We generate 200 clones with the orbital elements of QY1 within the 1σ range at the current epoch, considering their orbit covariances (quoted from the JPL Small-Body Database Browser site[2]). The applied orbital elements and their uncertainties are summarized in Table 6. We integrate these parameters to 8000 yr in the past with a time step of 8 days, considering the gravitational forces of the Sun and eight planets but ignoring the Yarkovsky force. As shown in Fig. 5, although the T_J values disperse before −1500 yr, there is a general trend that T_J values continue decreasing over time ($\Delta T_J \approx -0.1$ for 8000 yr). Based on this dynamic integration and our polarimetric results, QY1 would be an object of main-belt origin rather than outer Solar System origin. This result is consistent with the fact that S-complex asteroids are dominant in the 3:1 MMR (45%, Kuroda et al. 2014). For confirmation, we examine the possible source regions using the updated source region probability models (Greenstreet et al. 2012; Granvik et al. 2018) and find that QY1 has a high possibility (≈60%) of main-belt origin in 3:1 MMR and a very low probability (≈1–3%) of Jupiter-family comets origin using the updated orbital elements in Table 6.

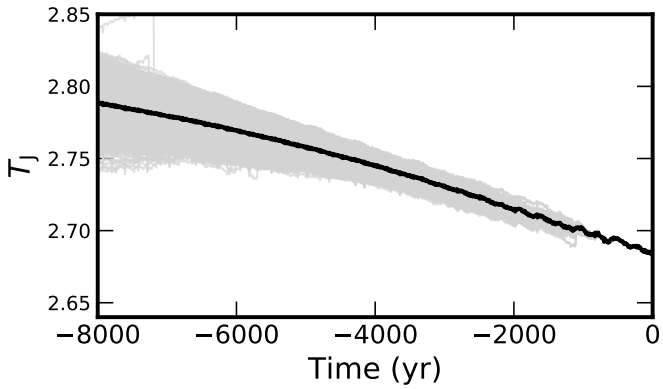

Fig. 5. Time evolution of the Tisserand parameter (T_J) with respect to Jupiter of QY1. T_J decreases by 0.1 over ~8000 yr, which supports that QY1 would be transported from the main-belt region. Each gray line represents different clones whose current orbital elements follow a Gaussian distribution around the average values within their standard deviations (Table 6). The black line represents the results for a particle with the average orbital elements at Epoch 2459396.5 (2021-07-01.0).

[2] https://ssd.jpl.nasa.gov/

4.4. Potentiality of polarimetry for ACO research

Finally, we describe the effectiveness of polarimetric observations in ACO research. The discrimination of dormant comets from the ACO population is challenging because both have a point-source appearance. The geometric albedos and reflectance spectra (or color indices) have been considered for discrimination. Comet nuclei have featureless and reddish colors due to irradiated organic materials on their surface (Meech et al. 2004; Licandro et al. 2011), while asteroids have a wide variety of colors (Tholen & Barucci 1989; Binzel et al. 2004). Similarly, comet nuclei have low albedos (typically p_V = 0.02–0.06, Campins & Fernández 2002; Lamy et al. 2004), while asteroids have a wide range of albedos (p_V = 0.02–0.60, Usui et al. 2011). D-type asteroids have optical properties similar to those of comet nuclei so they are indistinguishable by spectroscopic or photometric observation (DeMeo et al. 2009b; Licandro et al. 2011).

To date, geometric albedos of asteroids are derived mostly by radiometry. In the radiometric method, albedo values are derived from the combination of absolute magnitudes and sizes obtained via a thermal model with observation data. Accordingly, albedo values derived by radiometry have inherent uncertainties related to the applied thermal model and optical magnitudes. In addition, the use of mid-infrared observation facilities (e.g., space telescopes, such as AKARI, IRAS, and *Spitzer*, or ground-based telescopes with a mid-IR camera, such as SUBARU/COMICS) is becoming difficult (as of July 2021). On the other hand, because polarimetric instruments are less expensive than these infrared instruments, they are installed in a relatively large number of small and intermediate-sized telescopes. Using such instruments, albedo estimations, which were conventionally performed in infrared space telescopes or large telescope facilities on the ground, are possible. Since albedos can be obtained directly from polarimetric parameters using the empirical equation, no additional information is required (Widorn 1967; Kenknight et al. 1967; Cellino et al. 2012, 2015). Additionally, the constant parameters for deriving albedos from polarimetry continue to be updated and are becoming more reliable (Masiero et al. 2012; Cellino et al. 2015; Lupishko 2018). In addition, polarimetry with a polarizing beam splitter is highly feasible even under variable conditions, canceling out variable weather conditions to produce reliable results.

In the future it is expected that a large number of ACOs will be discovered by large systematic surveys, especially by the *Vera C. Rubin* Observatory (previously known as the Large Synoptic Survey Telescope, LSST; Vera C. Rubin Observatory LSST Solar System Science Collaboration 2021). Early follow-up polarimetric observations with a small or intermediate-sized telescope with a polarimetric instrument are expected to provide an overview of the dormant comet population lurking in the inner Solar System. Our work will be helpful in that we demonstrated the effectiveness and potentiality of polarimetry by conducting this ACO pilot survey for three objects.

5. Summary

We conducted a polarimetric pilot survey for three ACOs (Don Quixote, Hidalgo, and QY1). These three ACOs have a T_J value significantly smaller than three, and they were recognized as highly possible dormant comet candidates (Hartmann et al. 1987; Bottke et al. 2002). We obtain the polarization phase curve to conjecture their origins together with color information from previous studies. Our major findings are the following:

1. Don Quixote and Hidalgo show polarimetric and color profiles similar to those of comet nuclei and D-type asteroids. Their albedos derived by our polarimetric data are in the range of comet nuclei.
2. Our result of Don Quixote is consistent with the fact that the object indicated recurrent comet-like activities around its perihelion passages. Hidalgo is also likely a dormant comet.
3. The polarimetric profile of QY1 was unexpected, showing a profile similar to S-type asteroids. We find from the dynamical simulation that QY1 was transported from the main belt via the 3:1 mean motion resonance with Jupiter.
4. QY1 has $8.08^{+3.19}_{-3.11}$% in the V band and $8.14^{+3.41}_{-3.55}$% in the R_C band. From the P_{max} values we obtain an estimate of the particle diameter on the surface of QY1 of $d \approx 70$ μm.

The remaining issue is the polarimetric inversion angle (α_0). Hidalgo's α_0 is in the range of D-type asteroids and the active asteroid (7968) Elst-Pizarro, but out of 2P/Encke's range. Further polarimetric observations of comet nuclei and ACOs around the inversion angle are required to determine the inconsistency.

Acknowledgements. This work at Seoul National University was supported by the National Research Foundation of Korea (NRF), funded by the Korean government (MEST; No. 2018R1D1A1A09084105). The Pirka telescope is operated by the Graduate School of Science, Hokkaido University. The MITSuME telescopes at OAO and IAO are operated by the Tokyo Institute of Technology and the National Astronomical Observatory of Japan. Pirka and MITSuME are partially supported by the Optical & Near-Infrared Astronomy Inter-University Cooperation Program, MEXT, Japan. Part of the spectral data utilized in this publication was obtained and made available by the MIT-UH-IRTF Joint Campaign for NEO Reconnaissance. The IRTF is operated by the University of Hawaii under Cooperative Agreement no. NCC 5-538 with the National Aeronautics and Space Administration, Office of Space Science, Planetary Astronomy Program. The MIT component of this work is supported by NASA grant 09-NEOO009-0001 and by the National Science Foundation under Grants Nos. 0506716 and 0907766. Finally, we appreciate the anonymous reviewer for providing constructive and encouraging comments and suggestions.

References

Abell, P. A., Fernández, Y. R., Pravec, P., et al. 2005, Icarus, 179, 174
Astropy Collaboration (Robitaille, T. P., et al.) 2013, A&A, 558, A33
Astropy Collaboration (Price-Whelan, A. M., et al.) 2018, AJ, 156, 123
Bach, Y. P., Ishiguro, M., Jin, S., et al. 2019, J. Korean Astron. Soc., 52, 71
Bagnulo, S., Tozzi, G. P., Boehnhardt, H., Vincent, J. B., & Muinonen, K. 2010, A&A, 514, A99
Belskaya, I. N., & Shevchenko, V. G. 2000, Icarus, 147, 94
Belskaya, I. N., Shkuratov, Y. G., Efimov, Y. S., et al. 2005, Icarus, 178, 213
Belskaya, I. N., Fornasier, S., Tozzi, G. P., et al. 2017, Icarus, 284, 30
Binzel, R. P., Rivkin, A. S., Stuart, J. S., et al. 2004, Icarus, 170, 259
Boehnhardt, H., Tozzi, G. P., Bagnulo, S., et al. 2008, A&A, 489, 1337
Bottke, W. F., Morbidelli, A., Jedicke, R., et al. 2002, Icarus, 156, 399
Bottke, W. F., Vokrouhlický, D., Walsh, K. J., et al. 2015, Icarus, 247, 191
Bus, S. J., & Binzel, R. P. 2002, Icarus, 158, 146
Campins, H., & Fernández, Y. 2002, Earth Moon Planets, 89, 117
Campins, H., Ziffer, J., Licandro, J., et al. 2006, AJ, 132, 1346
Cellino, A., Gil-Hutton, R., Dell'Oro, A., et al. 2012, J. Quant. Spectr. Rad. Transf., 113, 2552
Cellino, A., Bagnulo, S., Gil-Hutton, R., et al. 2015, MNRAS, 451, 3473
Cellino, A., Bagnulo, S., Gil-Hutton, R., et al. 2016, MNRAS, 455, 2091
Cellino, A., Bagnulo, S., Belskaya, I. N., & Christou, A. A. 2018, MNRAS, 481, L49
Chambers, J. E. 1999, in Impact of Modern Dynamics in Astronomy, eds. J. Henrard, & S. Ferraz-Mello (Berlin: Springer), 449
Chernova, G. P., Kiselev, N. N., & Jockers, K. 1993, Icarus, 103, 144
DeMeo, F., & Binzel, R. P. 2008, Icarus, 194, 436
DeMeo, F., Binzel, R. P., Slivan, S. M., & Bus, S. J. 2009a, NASA Planetary Data System (USA: NASA), Bus-DeMeo Asteroid Taxonomy V1.0
DeMeo, F. E., Binzel, R. P., Slivan, S. M., & Bus, S. J. 2009b, Icarus, 202, 160
Dollfus, A., Wolff, M., Geake, J. E., Lupishko, D. F., & Dougherty, L. M. 1989, in Asteroids II, eds. R. P. Binzel, T. Gehrels, & M. S. Matthews (Tucson: University of Arizona Press), 594

Fernández, Y. R., McFadden, L. A., Lisse, C. M., Helin, E. F., & Chamberlin, A. B. 1997, Icarus, 128, 114
Fernández, Y. R., Jewitt, D. C., & Sheppard, S. S. 2001, BAAS, 33, 1093
Fernández, Y. R., Jewitt, D. C., & Sheppard, S. S. 2005, AJ, 130, 308
Fernández, Y. R., Campins, H., Kassis, M., et al. 2006, AJ, 132, 1354
Foreman-Mackey, D., Hogg, D. W., Lang, D., & Goodman, J. 2013, PASP, 125, 306
Fornasier, S., Belskaya, I., Shkuratov, Y., et al. 2006, A&A, 455, 371
Geake, J. E., & Dollfus, A. 1986, MNRAS, 218, 75
Gil-Hutton, R., Cellino, A., & Bendjoya, Ph. 2014, A&A, 569, A122
Gil-Hutton, R., López-Sisterna, C., & Calandra, M. F. 2017, A&A, 599, A114
Granvik, M., Morbidelli, A., Jedicke, R., et al. 2018, Icarus, 312, 181
Greenstreet, S., Gladman, B., Ngo, H., Granvik, M., & Larson, S. 2012, ApJ, 749, L39
Hartmann, W. K., Tholen, D. J., & Cruikshank, D. P. 1987, Icarus, 69, 33
Hasegawa, S., Marsset, M., DeMeo, F. E., et al. 2021, ApJ, 916, L6
Hsieh, H. H., & Jewitt, D. 2006, Science, 312, 561
Hsieh, H. H., Jewitt, D. C., & Fernández, Y. R. 2004, AJ, 127, 2997
Ishiguro, M., Nakayama, H., Kogachi, M., et al. 1997, PASJ, 49, L31
Ishiguro, M., Kuroda, D., Watanabe, M., et al. 2017, AJ, 154, 180
Ito, T., Ishiguro, M., Arai, T., et al. 2018, Nat. Commun., 9, 2486
Jewitt, D. C. 2002, AJ, 123, 1039
Jewitt, D. 2012, AJ, 143, 66
Kenknight, C. E., Rosenberg, D. L., & Wehner, G. K. 1967, J. Geophys. Res., 72, 3105
Kim, Y., Ishiguro, M., & Usui, F. 2014, ApJ, 789, 151
Kinoshita, D., Ohtsuka, K., Sekiguchi, T., et al. 2007, A&A, 466, 1153
Kokhirova, G. I., Ivanova, O. V., & Rakhmatullaeva, F. D. 2021, Sol. Syst. Res., 55, 61
Kresak, L. 1982, Bull. Astron. Inst. Czech., 33, 104
Kuroda, D., Ishiguro, M., Takato, N., et al. 2014, PASJ, 66, 51
Kuroda, D., Ishiguro, M., Watanabe, M., et al. 2015, ApJ, 814, 156
Kuroda, D., Geem, J., Akitaya, H., et al. 2021, ApJ, 911, 6
Lamy, P. L., Toth, I., Fernandez, Y. R., & Weaver, H. A. 2004, The Sizes, Shapes, Albedos, and Colors of Cometary Nuclei, eds. M. C. Festou, H. U. Keller, & H. A. Weaver (Tucson: University of Arizona Press), 223
Lamy, P. L., Toth, I., Groussin, O., et al. 2008, A&A, 489, 777
Lauretta, D. S., Hergenrother, C. W., Chesley, S. R., et al. 2019, Science, 366, 3544
Levison, H. F., & Duncan, M. J. 1997, Icarus, 127, 13
Levison, H. F., Terrell, D., Wiegert, P. A., Dones, L., & Duncan, M. J. 2006, Icarus, 182, 161
Li, J.-Y., Besse, S., A'Hearn, M. F., et al. 2013, Icarus, 222, 559
Licandro, J., Campins, H., Mothé-Diniz, T., Pinilla-Alonso, N., & de León, J. 2007, A&A, 461, 751
Licandro, J., Alvarez-Candal, A., de León, J., et al. 2008, A&A, 487, 1195
Licandro, J., Campins, H., Tozzi, G. P., et al. 2011, A&A, 532, A65
Licandro, J., Alí-Lagoa, V., Tancredi, G., & Fernández, Y. 2016, A&A, 585, A9
Lumme, K., & Muinonen, K. 1993, IAU Symp. 160, 194
Lupishko, D. F. 2014, NASA Planetary Data System (USA: NASA), EAR-A-3-RDR- 47 APD-POLARIMETRY-V8.0
Lupishko, D. F. 2018, Sol. Syst. Res., 52, 98
Masiero, J. R., Mainzer, A. K., Grav, T., et al. 2012, ApJ, 749, 104
Meech, K. J., Hainaut, O. R., & Marsden, B. G. 2004, Icarus, 170, 463
Mommert, M., Hora, J. L., Harris, A. W., et al. 2014, ApJ, 781, 25
Mommert, M., Trilling, D. E., Hora, J. L., et al. 2020, Planet. Sci. J., 1, 10
Morbidelli, A., Bottke, W. F., J., Froeschlé, C., & Michel, P. 2002, Origin and Evolution of Near-Earth Objects (Tucson: University of Arizona Press), 409
Nugent, C. R., Mainzer, A., Bauer, J., et al. 2016, AJ, 152, 63
Penttilä, A., Lumme, K., Hadamcik, E., & Levasseur-Regourd, A.-C. 2005, A&A, 432, 1081
Rayner, J. T., Toomey, D. W., Onaka, P. M., et al. 2003, PASP, 115, 362
Reach, W. T., Kelley, M. S., & Vaubaillon, J. 2013, Icarus, 226, 777
Shinnaka, Y., Kasuga, T., Furusho, R., et al. 2018, ApJ, 864, L33
Shkuratov, I. G., & Opanasenko, N. V. 1992, Icarus, 99, 468
Tancredi, G. 2014, Icarus, 234, 66
Tedesco, E. F., Noah, P. V., Noah, M., & Price, S. D. 2004, NASA Planetary Data System (USA: IRAS), IRASA-FPA-3-RDR-IMPS-V6.0
Tholen, D. J. 1984, PhD thesis, University of Arizona, Tucson, USA
Tholen, D. J., & Barucci, M. A. 1989, in Asteroids II, eds. R. P. Binzel, T. Gehrels, & M. S. Matthews (Tucson: University of Arizona Press), 298
Tinbergen, J. 1996, Astronomical Polarimetry (Cambridge: Cambridge University Press)
Tubiana, C., Barrera, L., Drahus, M., & Boehnhardt, H. 2008, A&A, 490, 377
Umow, N. A. 1905, Physics, 6, 674
Usui, F., Kuroda, D., Müller, T. G., et al. 2011, PASJ, 63, 1117
Usui, F., Kasuga, T., Hasegawa, S., et al. 2013, ApJ, 762, 56
van Dokkum, P. G. 2001, PASP, 113, 1420
Vera C. Rubin Observatory LSST Solar System Science Collaboration, Jones, R. L., Bannister, M. T, et al. 2021, BAAS, 53, 236
Wardle, J. F. C., & Kronberg, P. P. 1974, ApJ, 194, 249
Warner, B. D., & Benishek, V. 2016, Minor Planet Bull., 43, 285
Watanabe, M., Takahashi, Y., Sato, M., et al. 2012, Proc. SPIE, 8446, 84462O
Weissman, P. R., Bottke, Jr. W. F., & Levison, H. F. 2002, Evolution of Comets into Asteroids, ed. W. F. Bottke, Jr., A. Cellino, P. Paolicchi, & R. P. Binzel (Berlin: Springer), 669
Widorn, T. 1967, Annalen der Universitaets-Sternwarte Wien, Dritter Folge, 27, 109
Willmer, C. N. A. 2018, ApJS, 236, 47

Appendix A: Usage of the terms comets and asteroids

Here we describe the designations of comets and asteroids adopted throughout this paper.

Comets and asteroids have been distinguished from several viewpoints (such as their appearance, composition, and orbital properties). If a small body of the Solar System indicates activity accompanied by a coma and a tail, it is conventionally regarded as a comet; otherwise, it is regarded as an asteroid. From their composition, asteroids consist mostly of refractory components with a small amount of volatiles (or without volatiles), while comets are rich in volatile components and refractory components.

Comets and asteroids are also distinguished by their orbital properties. Comets are thought to migrate from the outer Solar System (i.e., the Kuiper Belt or the Oort Cloud) via dynamic interactions with Jovian planets, and to exhibit comet-like activities when they receive extra solar radiation that causes ice sublimation to form comae and tails. Such objects from the outer Solar System intersect with Jovian planets and have Tisserand parameter values $T_J < 3$. On the other hand, asteroids are dynamically disconnected from Jovian planets and have $T_J > 3$ (Levison & Duncan 1997).

These comet-asteroid discrimination methods do not always work, however. For example, 2P/Encke contains icy volatiles (e.g., H_2O and CO_2, Reach et al. 2013) showing regular activity, but has the Tisserand parameter $T_J = 3.03$ (i.e., an asteroidal orbit). It is considered that 2P/Encke has the current asteroidal orbit due to the nongravitational effect (acceleration by sublimation of ice) and the gravitational interaction with planets (Levison et al. 2006). Furthermore, after discovering the so-called main-belt comets (comets in the main asteroidal belt with $T_J > 3$), the distinction between comets and asteroids became ambiguous (Hsieh & Jewitt 2006). The recent discovery of very red asteroids (similar to Kuiper Belt objects) further complicates the designations (Hasegawa et al. 2021).

We were motivated to study ACOs by pioneering research: Fernández et al. (1997), DeMeo & Binzel (2008), Licandro et al. (2008), and Kim et al. (2014). ACOs are asteroids with comet-like orbits ($T_J < 3$), and most ACOs are thought to be dormant (or low activity) comets that are at the last stage of the evolution of the bodies from the Kuiper Belt or the Oort Cloud, although there are some asteroids transported to the current orbits via mechanisms such as the Yarkovsky effect (Morbidelli et al. 2002; Kim et al. 2014). Since the purpose of this study is to distinguish comets from ACOs, throughout this paper we refer to objects originating from or in the main belt as asteroids and objects from the Kuiper Belt or the Oort Cloud as comets.

Appendix B: Photometry of QY1

We conducted these observations to detect a signature of comet-like activity. A series of photometric observations were made at three observatories: the Okayama Astrophysical Observatory (OAO), the Ishigakijima Astronomical Observatory (IAO), and the Observatoire de Haute-Provence (OHP). The detailed circumstances of the observations are given in Table B.1.

The OAO is located atop Mt. Chikurinji, Okayama Prefecture, Japan (133°35′36″E, 34°34′33″N, 360 m). We performed observations on three nights on UT May 2–5, 2016, using the Multicolor Imaging Telescopes for Survey and Monstrous Explosions (MITSuME) with three Alta U6 cameras (1024 × 1024 pixels) attached to the 50 cm telescope. The IAO is located on Ishigaki Island, Okinawa Prefecture, Japan (124°08′21.″4 E, 24°22′22.″3 N, 197 m). We observed the target asteroid for seven nights on UT May 26–June 12 2016. We used the 105 cm Murikabushi Cassegrain telescope and MITSuME. The MITSuME at IAO was identical to the system at OAO. The OHP is located in Alpes-de-Haute-Provence, Saint-Michel-l'Observatoire, France (5°42′48″E, 43°55′51″N, 650 m). We made observations on three nights on UT August 1–3 2016. We utilized a 120 cm telescope (focal length of 7.2 ,m) and an Andor Ikon L 936 camera (2048 × 2048 pixels). The fields of view and pixel scales of these instruments are 12.′3 × 12.′3 (0.″72 pixel^{-1}) at IAO, 26.′0 × 26.′0 (1.″53 pixel^{-1}) at OAO, and 13.′1×13.′1 (0.″38 pixel^{-1}) at OHP.

We note that all of these images show a point-like target without showing a comet-like coma and tail. The brightness modulation by rotation was detected, as shown below. The observed raw magnitudes were converted into magnitudes viewed at heliocentric and geocentric distances of $r_h = \Delta = 1$ au and a phase angle of $\alpha = 70°$,

$$m_R\,(70°) = m_R - 5\ \log_{10}(r_h\Delta) + b\,(\alpha - 70°)\ \ , \tag{B.1}$$

where the phase coefficient of $b = 0.032$ was assumed, which is a predicted value for an object with $p_V = 0.178$ (see the empirical equation on page 99, Belskaya & Shevchenko 2000).

We made a plot of the light curve applying the rotation periods in Warner & Benishek (2016), where two rotational periods are suggested: $P_1 = 45.5$ hours and $P_2 = 36.6$ hours (Fig. B.1). P_1 is the best candidate of the main period. The uncertainty of the period of 0.5 hours is quoted. From our light curve data, the modulation of P_1 is clearly seen, but the modulation of P_2 is not, probably because our amount of data may not be sufficient to find it.

The observations at OHP was conducted approximately two months after the observations at OAO and IAO. The accuracy of the rotational period (0.5 hours) is not sufficient to compare the OHP data with the others, so we do not plot the OHP data in Fig. B.1. The magnitudes at OHP, $m_R(70°) = 17.20$–17.65 mag, are in the range of the maximum and minimum magnitudes in Fig. B.1, so it is likely that the phase angle correction with b works well for the OHP data. This supports the validity of our estimate for the geometric albedo. The reduced magnitude of QY1 in Fig. B.1 is available at the CDS.

Appendix C: Derivation of spectral gradients in Fig. 4

In Sect. 3.3 we plotted the polarimetric slope h and the color index $V - R$ for three ACOs, asteroids, and comet nuclei (Fig. 4). We used the h values of asteroids provided in the catalog of the asteroid polarization curves (Gil-Hutton et al. 2017). The applied slope h values from the catalog are determined in the V band. Because of the lack of h data for D-type asteroids, we computed h values from p_V values of 267, 1542, 2246, 2569, 2872, 3248, and 4744 by Eq. (7). The albedos of these D-type asteroids are obtained from Usui et al. (2011), Nugent et al. (2016), and Tedesco et al. (2004). If there is multiple albedo information in these catalogs, the averaged values are calculated and used for the plot. The $V - R$ of asteroids and ACOs are derived using the Small Main-Belt Asteroid Spectroscopic Survey (SMASS) data (Bus & Binzel 2002; Rayner et al. 2003). From SMASS spectra, we calculated the normalized spectral gradient (S') defined as

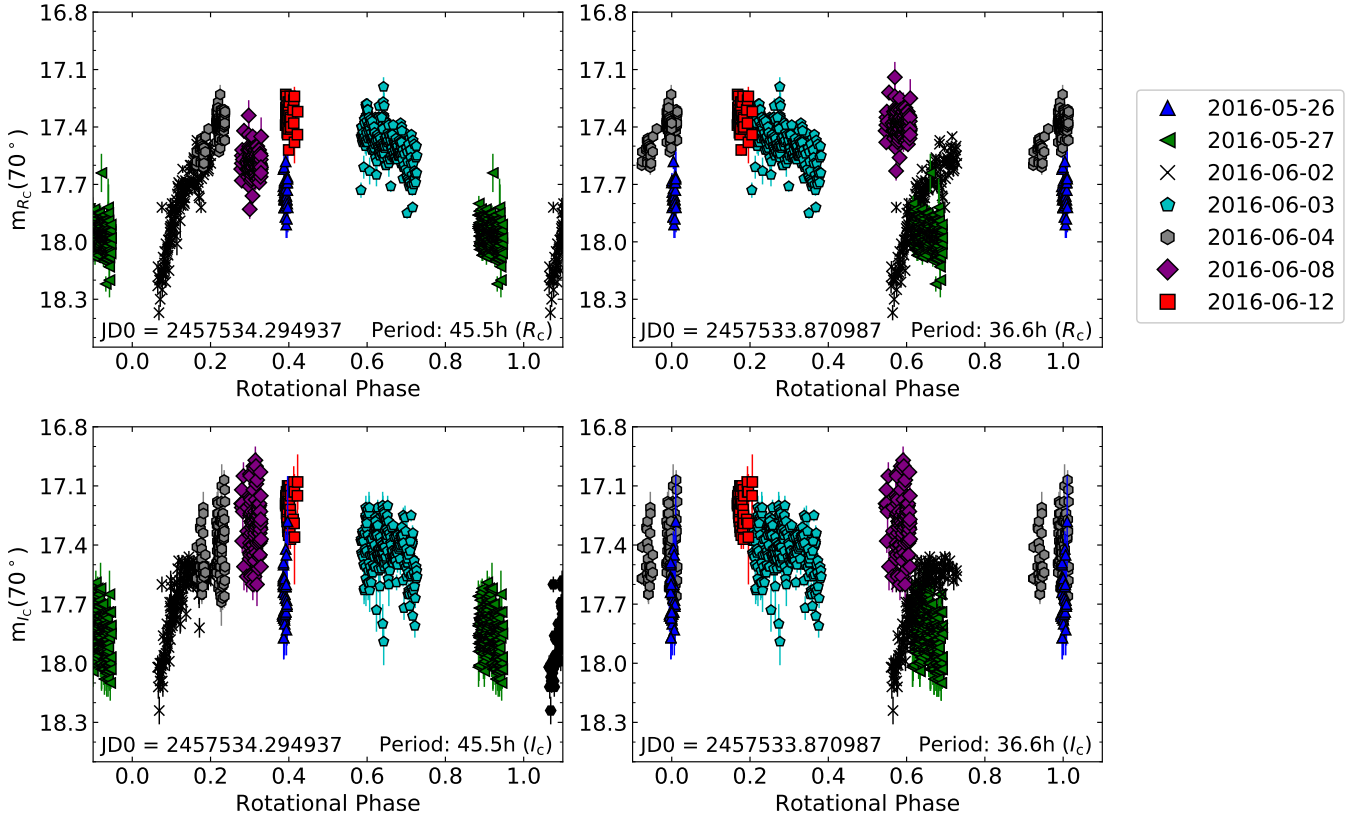

Fig. B.1. Light curves of R_C band (top) and I_C band (bottom) produced assuming a rotational period of P_1 = 45.5 hours (left column) and P_2 = 36.6 hours (right column) (see Warner & Benishek 2016). The horizontal axes indicate the rotational phase, and the vertical axes indicate the magnitudes viewed from $r_h = \Delta = 1$ au at $\alpha = 70°$, assuming a phase slope parameter $b = 0.032$ mag/deg.

Table B.1. Observation circumstance of photometric data

Date	UT	Telescope	Filter	Exptime[a] (sec)	N^b	r^c (au)	Δ^d (au)	α^e (deg)
2016-May-26	12:33–13:09	IAO	g', R_C, I_C	30	76	0.88	0.29	108.6
2016-May-27	11:15–14:03	IAO	g', R_C, I_C	20	476	0.90	0.28	105.0
2016-Jun-02	11:39–17:48	OAO	g', R_C, I_C	120	320	1.01	0.28	82.1
2016-Jun-02	13:05–14:17	IAO	g', R_C, I_C	20	18	1.01	0.28	82.2
2016-Jun-03	11:14–17:43	OAO	g', R_C, I_C	120	350	1.03	0.29	78.5
2016-Jun-03	11:47–17:16	IAO	g', R_C, I_C	20	384	1.03	0.29	78.5
2016-Jun-04	13:34–16:58	IAO	g', R_C, I_C	20	222	1.05	0.29	75.1
2016-Jun-05	11:47–16:20	OAO	g', R_C, I_C	120	164	1.07	0.30	72.0
2016-Jun-08	13:34–15:52	IAO	g', R_C, I_C	20	262	1.12	0.33	63.4
2016-Jun-12	13:31–14:55	IAO	g', R_C, I_C	20	82	1.19	0.38	54.8
2016-Aug-01	20:50	OHP	R_C	300	1	1.90	1.39	31.3
2016-Aug-02	20:23–20:29	OHP	R_C	300	2	1.91	1.41	31.2
2016-Aug-03	20:09–20:19	OHP	R_C	300	3	1.92	1.43	31.0

Notes. The observation circumstance of light curve data taken at Okayama Astrophysical Observatory (OAO) and Ishigakijima Astrophysical Observatory (IAO). We used the web-based JPL Horizons system (`http://ssd.jpl.nasa.gov/?horizons`) to obtain these quantities. [a]Exposure time in sec, [b]Number of data obtained, [c]Median heliocentric distance in au, [d]Median geocentric distance in au, [e]Median solar phase angle in deg.

$$S' = \left(\frac{dS}{d\lambda}\right) \Big/ \overline{S} \ , \tag{C.1}$$

where S is the λ-dependent reflectance, and $\overline{S}$ is the average S in the wavelength range of $d\lambda$. Here the $dS/d\lambda$ values were calculated by the linear fitting of SMASS spectra between 5 500 Å and 6 500 Å. The derived S' values were converted to $V-R$ values by using Eq. (2) in Jewitt (2002). We obtained $V - R = 0.49 \pm 0.01$ for Don Quixote and $V - R = 0.48 \pm 0.01$ for Hidalgo.

Because there is no optical spectrum for QY1, we derived it using our photometric data (g'-, R_C-band). The value of S' of QY1 is derived as

$$\log_{10}(S_\lambda) = \frac{m_\lambda - m_{\odot,\lambda}}{-2.5} \tag{C.2}$$

and

$$S' = \left(\frac{S_{R_C} - S_{g'}}{\lambda_{R_C} - \lambda_{g'}}\right) \Big/ \left(\frac{S_{R_C} + S_{g'}}{2}\right) , \tag{C.3}$$

where the subscript λ denotes the effective wavelength of filters, and m_λ and $m_{\odot,\lambda}$ are the apparent magnitudes of the object and the Sun at wavelength λ, respectively. Here, we use $m_{\odot,R_C} = -27.15$ mag and $m_{\odot,g'} = -26.34$ mag (Willmer 2018) and $\lambda_{R_C} = 6\,480$ Å and $\lambda_{g'} = 4\,710$ Å. With these parameters we derived the $V - R$ of QY1 as $V - R = 0.46 \pm 0.03$.

Similarly to the D-type asteroids, the slope h values of comet nuclei were computed from their albedos. The geometric albedos and $V - R$ (or S') of comet nuclei were obtained from various sources (Jewitt 2002; Meech et al. 2004; Abell et al. 2005; Campins et al. 2006; Fernández et al. 2006; Lamy et al. 2008; Tubiana et al. 2008; Li et al. 2013). For 2P/Encke and (7968) Elst-Pizarro, we referred to the slope h values in Boehnhardt et al. (2008) and Bagnulo et al. (2010).